JOURNAL OF MATERIALS SCIENCE **40** (2005) 3735–3743

YSZ electrolyte of anode-supported SOFCs prepared from sub micron YSZ powders

M. GAUDON, N. H. MENZLER*
Forschungszentrum Jülich, Institute for Materials and Processes in Energy Systems (IWV-1), 52425 Jülich, Germany
E-mail: n.h.menzler@fz-juelich.de

E. DJURADO
Laboratoire d'Electrochimie et de Physico-chimie des Matériaux et des Interfaces (LEPMI), 1130 Rue de la piscine, 38402 St. Martin D'Hères, France

H. P. BUCHKREMER
Forschungszentrum Jülich, Institute for Materials and Processes in Energy Systems (IWV-1), 52425 Jülich, Germany

Dense and thin electrolytes composed of yttrium-stabilized zirconia for anode-supported solid oxide fuel cells were produced by slip casting of different powder suspensions. These suspensions were obtained by mixing different proportions of nanocrystalline powder made by spray pyrolysis and commercial micro-sized powder in ethanol. Two parameters influence mostly the formation of gastight thin films: the powder morphology which controls the green density of the films and the powder sintering activity on which depends the formation of cracks during drying and sintering and adhesion. Here, optimized powder mixtures allowed the formation of a 5 μm thick electrolyte with efficient gastightness besides industrial applications. It is shown in this study that the optimum suspension composition corresponds to the best compromise between powder morphology and powder sintering activity.

1. Introduction

One of the most important components of the solid oxide fuel cell (SOFC) is the solid electrolyte. For SOFC electrolyte, stabilised cubic zirconia with 8 mol% yttrium oxide (8YSZ) is still the essential material because it has sufficient ionic conductivity at planar SOFC operating temperatures (about 10^{-2} S $\cdot$ cm^{-1} at 800°C) [1, 2], it is stable under oxidising and reducing atmospheres and it is compatible with a perovskite cathode ((La,Sr)MnO_3 or (La,Ca)MnO_3) from the chemical (no solid-state reaction) and mechanical (coefficient of thermal expansion) points of view [3, 6]. However, it is very important to reduce YSZ thickness as much as possible (e.g. <10 μm) in order to decrease ohmic losses through the electrolyte and to lower the SOFC operating temperature [7, 8]. This reduction of the electrolyte thickness must not affect the gastightness of the layer. Indeed, a gastight electrolyte is required to ensure that the two reactive gases (e.g. air and hydrogen) do not mix since this would lead to a decrease in the hydrogen conversion efficiency, the open circuit voltage and thus in the final power density of the cell. Quantitatively it was considered, in particular on the basis of findings from Siemens-Westinghous, that gastightness corresponding to an air leakage rate through the electrolyte of about 10^{-4} mbar.l.s^{-1} $\cdot$ cm^{-2} is required [9]. At Research Centre Jülich, a slurry process (elsewhere called the vacuum slip casting process) is used to obtain thin electrolytes on a porous substrate [10–12]. In this process the slurries are prepared from micro-sized powder (8YSZ from Tosoh corporation) pre-sintered at about the same temperature as the substrate (1240°C). If the powders and substrate are pre-sintered at the same temperature, the differences in shrinking rate between the material of the porous substrate and the electrolyte film material can be carefully matched [13, 14]. Using this process, electrolyte layers of sufficient gastightness can be obtained with a thickness >10–15 μm [15]. In this paper, perfectly spherical powder with nano-sized grains, prepared by the spray pyrolysis process, were used to obtain 5-μm-thick layers with sufficient gastightness. It has to be noted that, even if some studies in the literature have shown that pellets with very high density can be achieved at relatively low sintering temperatures using nano-sized powder [16, 17], for the manufacture of YSZ electrolyte on anode-supported cells, nano-sized powders have already been used but have not achieved adequate results [18, 19]. In fact, during co-firing of a layer on a substrate, the high sintering activity at low temperature of nano-sized powder

*Author to whom all correspondence should be addressed.

leads to a strong mismatch between the substrate and the layer shrinkage, and thus leads to the propagation of cracks and/or layer delamination [13, 14]. In this paper, a possible solution to this problem by using different slurry mixtures of micro-sized and sub micron-sized powders is presented.

2. Experimental

2.1. Powder materials

Two raw powders, which could also be pre-sintered at different temperatures, were used in this study. The pre-sintering temperature directly controls the crystallite size of the powder and so, influences their sintering activity. Thus, by enhancing the pre-sintering temperatures of the powders used in the layers to be coated, parameters as final densification, crack propagation during drying and sintering, and adherence of the layers will be affected.

The micro-sized powder is a commercially available 8YSZ powder: 8 mol% yttrium-stabilised zirconia (Tosoh Company, Japan). The grain size of this powder increased from about 50 nm after a calcination step at 800°C to 250–300 nm after a sintering step at 1240°C [20]. A sub micron-sized powder, of the same 8YSZ composition, was produced by spray pyrolysis. A full description of the process is given in Djurado *et al*. [21]. Briefly, the 8YSZ zirconia powder was prepared from precursor solutions consisting of a stoichiometric mixture of zirconyl nitrate hydrate $ZrO(NO_3)_2 \cdot 6H_2O$ and yttrium nitrate hydrate $Y(NO_3)_3 \cdot 6H_2O$ dissolved in distilled water. These solutions were atomised by a high-frequency ultrasonic mist generator with a piezoelectric ceramic transducer, for which a frequency of 1.7 MHz was used in this work. The aerosol produced was carried through a tubular furnace in an air (N_2-O_2 mixture) flow rate of $6l \cdot min^{-1}$and the temperature of the tubular furnace was fixed at 600°C. The microstructure of the powder used in the raw state or after pre-calcination at 800°C was investigated by X-ray diffraction (XRD), helium pycnometry and scanning electron microscopy (SEM).

2.2. Slurry preparation

In both cases to form a stable slurry the powders were ball milled in polyethylene bottles with zirconia balls (8YSZ, 3 mm diameter) on a rolling bank for 24 h. The solvent used was ethanol and polyethyleneimine was added as a dispersing agent. Slurries of different wt% of micro-sized and sub micron-sized powders were prepared. In the following, a layer prepared from a slurry containing X wt% of micro-sized powder and 100-X wt% of sub micron-sized powder is called the [X/1-X] layer.

2.3. Layer deposition and co-firing process

The suspensions were deposited by slurry coating on pre-sintered porous NiO-YSZ substrates fabricated by the Coat-Mix® process [22, 23]. Before slurry coating, the substrates were already coated with an anode pre-calcined at 1000°C [22]. The thickness of the electrolyte layer was adjusted by controlling the powder wt% of the suspensions and the volume of the suspensions used, taking into account the pre-sintered substrate area and the substrate area shrinkage during co-firing treatment. Except for green layer density calculations, only 5 μm thick layers (thickness after sintering) were prepared in this study. Co-firing treatment of the total half-cell assembly was performed at 1400°C for 5 h with a heating rate of $180°C \cdot h^{-1}$ in air. Finally a reduction step to convert the nickel oxide component to metallic nickel in the substrate and the anode was performed at 900°C for 10 h with a heating rate of $100°C \cdot h^{-1}$ in Ar + 4% H_2.

2.4. Characterisation techniques

The crystallographic structure of the sprayed powder was characterised by X-ray diffraction using a Siemens D-500 diffractometer. The grain sizes were evaluated from XRD patterns by applying the Scherrer formula. Particle density was measured with a double room helium pycnometer (Micromeritics-AccuPyc 1330). Calculations were then carried out using the ideal gas law (accuracy for particle density was estimated to be about 1%). The degree of dispersion of both powders (spray pyrolysed or Tosoh powders) in slurries was analysed using a laser Shimadzu SA-CP3 granulometer; only cumulative particle size distributions (in count) are presented in this work. Powder or layer morphology was examined using a scanning electron microscope (Jeol JSM 6400). In addition, the sintering behaviour of 8mm pellets made from different powder mixtures uniaxially pressed ($P = 300$ MPa) was studied by dilatometric analyses. Glycerine was used as binder; the total amount of glycerine was adapted to obtain approximately the same green density for pellets of each composition. The sintering curves were recorded using a push-rod dilatometer Netzsch 402 E. The sintering step was performed at 1400°C for 5 h with a heating rate of $180°C \cdot h^{-1}$ (same conditions as for the co-firing step). The final densities of the pellets were calculated from final mass/final volume ratio. The gastightness of the electrolyte layers was characterised by gas leak rate measurements. Gas leak rates through the electrolyte membranes (abbreviated to GLR in the figures) were measured at room temperature using a Balzers QualiTest 265 helium leak finder. The sample to be measured is placed with the electrolyte side on the bottom on a squared rubber seal lying on a perforated metal plate. The metal plate is the top of a vacuum chamber. After applying the sample vacuum is drawn from the bottom side. After a stable vacuum helium gas is applied on the top of the sample. A mass spectrometer is now detecting the amount of helium migrating through the half cell coated with the gastight electrolyte. The gas leak rate is calculated taking into account the pressure difference on the vacuum side and on the air side, the time, the volume of the vacuum chamber and the measured area. Thus the GLR is designated in mbar l/s cm^2. Here, only average gas leak rates are discussed. The average values are calculated from measurements made on at least on 5 samples.

3. Results and discussion

3.1. Layers made from only micro-sized powder

As was mentioned in the Introduction, at Research Centre Jülich, electrolyte layers are classically made from Tosoh powder pre-sintered at 1240°C (Tosoh 1240). Here, for comparison with the following studies, the particle size distribution of a ball-milled Tosoh slurry, the morphologies of typical green and co-fired 5 μm thick layers, and the gas leak rate through this co-fired layer were studied. As can be seen from the granulometric curve performed on a Tosoh suspension (see Fig. 1), the particle size distribution is centred on 0.5 μm ($d_{50} = 0.51$ μm). Furthermore, this distribution is rather sharp: the d_{95} diameter is around 3.5 times the d_{05} diameter. On the green layer top view (shown in Fig. 2a), the surface is obviously rather rough. It seems difficult to obtain a good thickness homogeneity, which may explain the difficulties in obtaining a dense and rather thin layer using Tosoh material. For co-fired 5 μm layers analysed after the reduction of the substrate, a lot of open pores with variable diameters are detected by SEM investigations of the layer surface (Fig. 2b). The gas leak rate average value for 5-μm-thick layers made of Tosoh powder (20 samples were tested) is about 2×10^{-3}mbar $\cdot 1 \cdot s^{-1} \cdot cm^{-2}$, (variation between 8×10^{-4} and 5×10^{-3}mbar $\cdot 1 \cdot s^{-1} \cdot cm^{-2}$) i.e., one order of magnitude higher than the required value.

3.2. Layers made from only sub micron-sized powder

Before the preparation of electrolyte layers from slurries of pure sub micron-sized YSZ powder are presented, the characteristics of this powder have to be described. The raw spray pyrolysis powder consists of perfectly spherical particles containing primary crystallites. An SEM picture of this powder is presented in Fig. 3. In a previous publication [24], it was shown that the spherical particles of the raw spray pyrolysis powder are not completely dense. To achieve a complete densification of the spherical particles, it was found here that the spray pyrolysis powder has to be pre-calcined at 800°C. Indeed, helium picnometry measurements performed on raw material and material calcined at 800°C showed densities equal to 4.75 g $\cdot$ cm^{-3} and 5.65 g $\cdot$ cm^{-3}, respectively, i.e. ≈80% and 95% of the oxide theoretical density (taking a theoretical density of 5.96 $g \cdot cm^{-3}$for 8YSZ oxide). The low calcination temperature is sufficient to suppress the closed porosity inside spherical particles but not to start the sintering of these spherical particles (no necks were formed between the particles). This densification phenomenon at such low temperature can be explained by the sub micron-sized spherical particles consisting of basic nano-sized crystallites. The smallness of the crystallites seems to be the

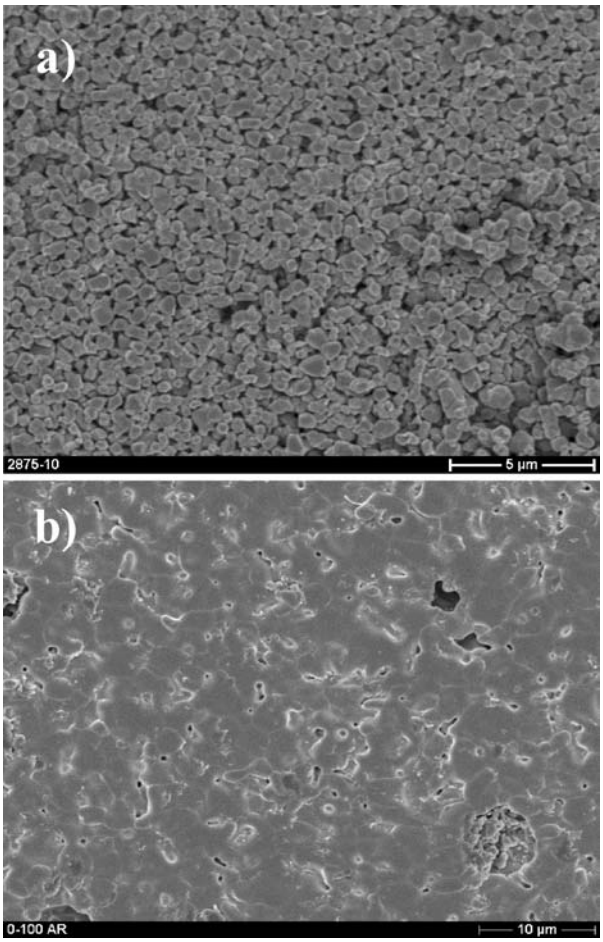

Figure 2 SEM top views of (a) green Tosoh 1240 layer and (b) sintered Tosoh 1240 layer.

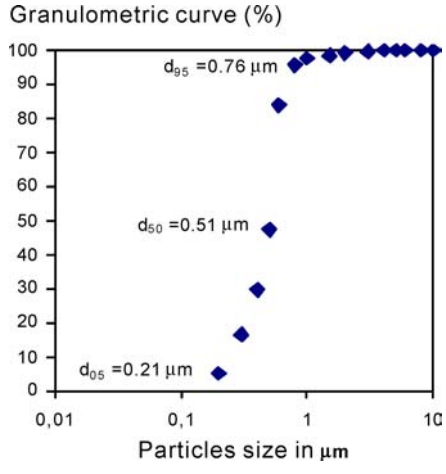

Figure 1 Cumulative distribution (in %) of ethanol slurry of sintered Tosoh at 1240°C (Tosoh 1240).

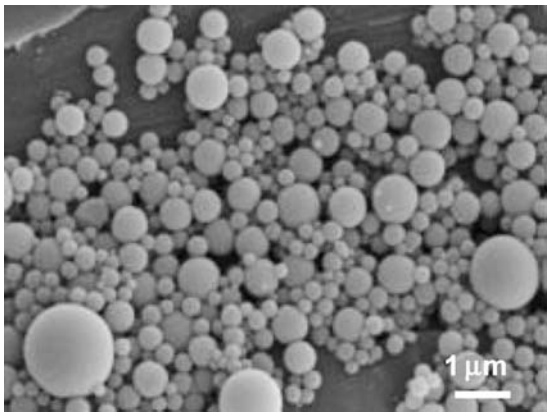

Figure 3 SEM picture of the spray pyrolysis powder (raw material).

cause of the reorganisation of the matter inside the particles calcined at 800°C. Indeed, XRD studies on raw and calcined powders have shown that the nano-sized crystallites grow from 4.6 nm to 10.6 nm during calcination, i.e. a multiplication of the crystallite size by more than a factor of two. However, a total absence of changing for the polycrystalline particle morphology was observed (no neck formation between polycrystalline particles). Otherwise, XRD patterns presented in Fig. 4 also confirm that spray pyrolysis powders are crystallised in a pure cubic phase.

A granulometric distribution (characteristic of the polycrystalline particles) calculated by image analysis of the SEM micrograph of raw spray pyrolysis powder is shown in Fig. 5. (due to the small particle sizes the measurements by laser particle size analyser show agglomeration even after applying ultrasonic). The image analysis was made using the software ImageTool; about 500 particle diameters were measured for the granulometric curve. The average diameter is about 0.32 μm. As could be assumed from the SEM micrograph, spray pyrolysis powder presents a rather wide particle size distribution, wider than for the Tosoh ball-milled powder in suspension (here, the difference factor between d_{95} and d_{05} is more than 5). It has to be added that the densification caused by the pre-calcination of spray powders has too small an impact on the spherical particle diameters to be detected by granulometric measurements (theoretically, a densification of 15% leads to a diameter decrease of about 5%). It can thus be considered that the granulometric distribution of the pre-calcined powder is almost the same as the raw powder presented in Fig. 5.

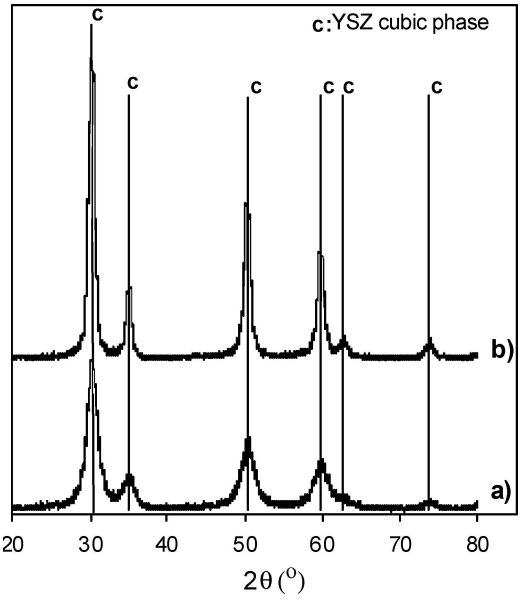

Figure 4 XRD patterns of (a) raw spray powder and (b) 800 spray powder.

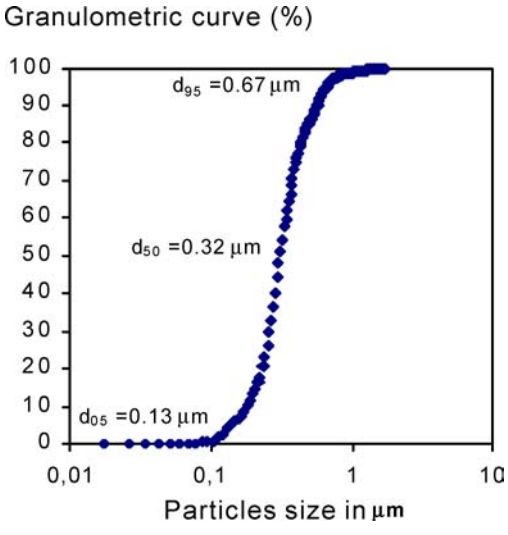

Figure 5 Cumulative distribution (in %) of raw spray powder obtained by image treatment of the SEM picture.

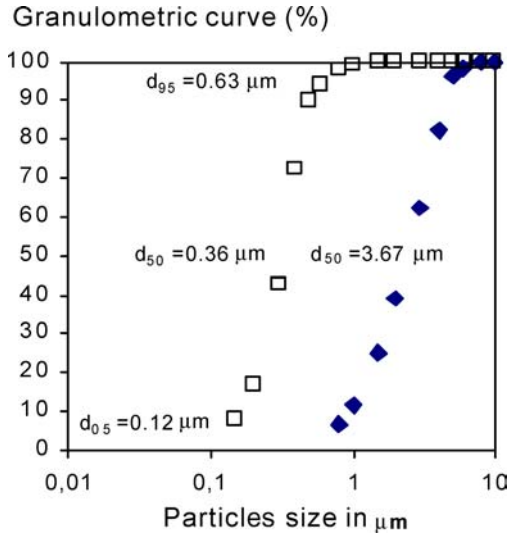

Figure 6 Cumulative distribution (in %) of slurries of raw spray powder (filled rhombuses) and of spray powder pre-calcined at 800°C (800 spray powder).

Two suspensions of raw and calcined powders were prepared. The granulometric distributions of powders inside the suspensions after the ball-milling step are presented in Fig. 6. It can be seen that the suspension of the raw powder presents large agglomerates ($d_{50} \approx 4$ μm), whereas the suspension of calcined powder presents a cumulative particle size distribution more or less similar to that calculated from the SEM micrograph ($d_{50} \approx 0.36$ μm). It is assumed that the ability to disperse the calcined powders but not the raw powder is based on the lowering of the surface energy of the spherical particles due to the increase of the grain sizes. The two prepared slurries were deposited on NiO-YSZ substrates by the slurry coating process. Micrographs of green layers resulting from these depositions are presented in Fig. 7. The agglomeration of the raw powder inside the precursor slurry leads to very rough layers (Fig. 7a), whereas the good dispersion of the calcined spray powders allows the production of very smooth and homogeneous layers (Fig. 7b). Micrographs of both layers after the co-firing step are presented in same figure. Raw powder leads to sintered layers with large cracks (Fig. 7c), whereas layers made of calcined powder present only a few narrow cracks (Fig. 7d). The average gas leak rate values were found to be between 3×10^{-1} and 1×10^{-3} mbar $\cdot$ l $\cdot$ s^{-1} $\cdot$ cm^{-2}, respectively. At least three benefits could be obtained by pre-calcination

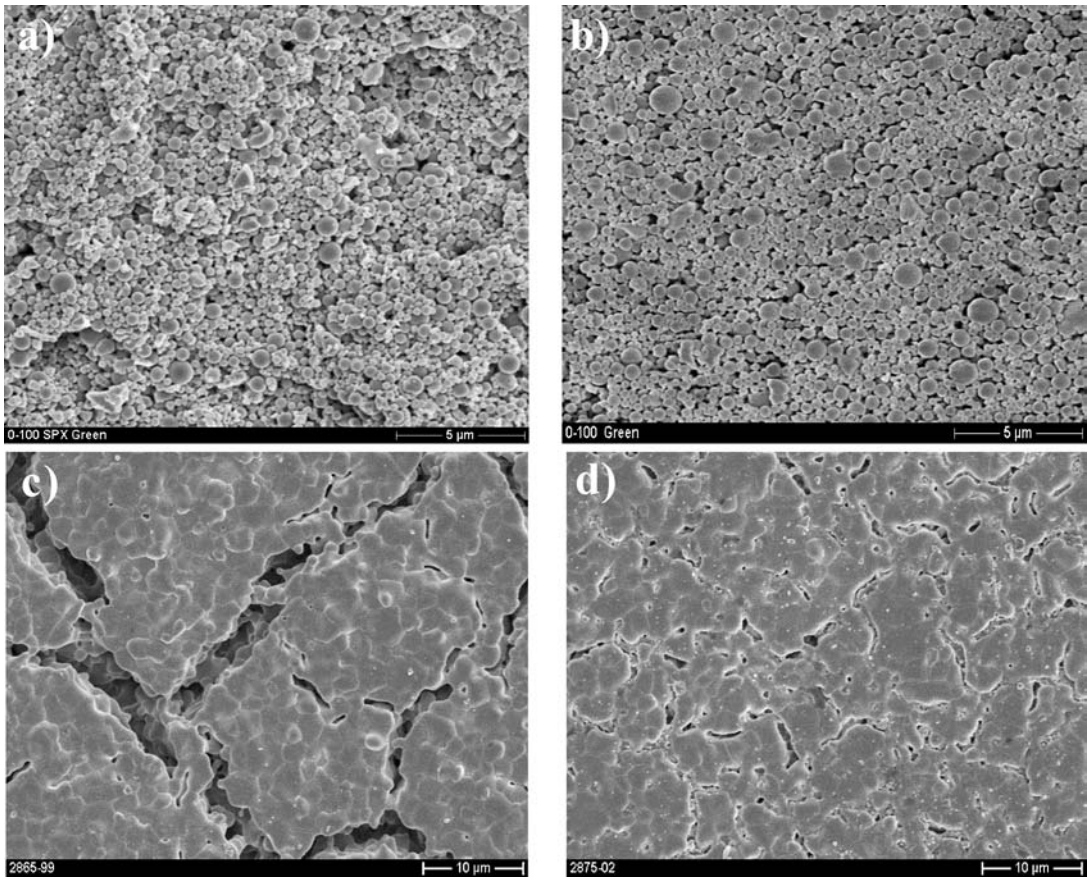

Figure 7 SEM top views of green layers made of (a) raw spray powder, (b) 800 spray powder and of sintered layers made of (c) raw spray powder, (d) 800 spray powder.

of the spray pyrolysis powder before dispersing it in the precursor slurry. Firstly, better green layer morphology (higher green density) is achieved because of the good dispersion of the powder in suspension. Secondly, the calcined powder particles are denser than the raw ones, and green layers are easier to densify. Thirdly, the sintering activity of the calcined powder at low temperature is reduced in comparison to the raw powder and thus the thermal mismatch between the layer and the substrate is reduced as is the shrinkage. However, using pure calcined spray powders for the preparation of 5-μm-thick layer is still not efficient for obtaining sufficient gastight layers under these experimental conditions. Indeed, the gas leak rates of sintered layers made of such powder are too high for industrial applications. This non-satisfactory result undoubtedly comes from a mismatch between the layer and the substrate shrinkage.

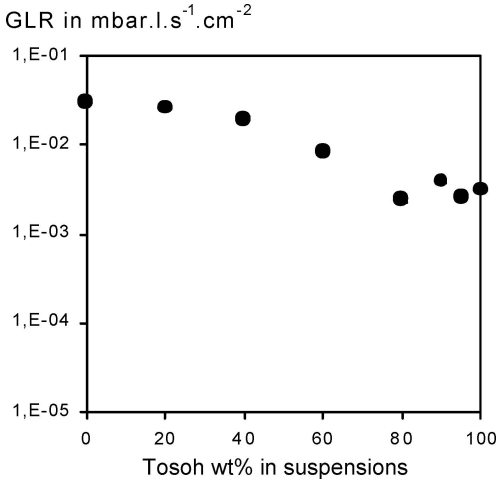

Figure 8 Helium leak rates of sintered layers made of raw spray powder/Tosoh 1240 powder mixtures.

3.3. Layers made of micro-sized/sub micron-sized powder mixtures

Despite the inadequate results obtained from pure raw spray pyrolysis powder, for comparison with the next study, layers of mixtures of raw spray pyrolysis powder and Tosoh powder (pre-sintered at 1240°C) were prepared. The gas leak rates of co-fired layers from different mixtures are presented in Fig. 8. It can be seen that no improvement in gastightness was found for "composite" layers in comparison with layers from pure Tosoh powder. In a parallel manner, gastightness of layers prepared from mixtures of pre-calcined spray pyrolysis powder and Tosoh powder were also analysed by leak rate measurements which are shown in Fig. 9. Here, in contrast to the previous study, a strong improvement in gastightness was obtained for some mixtures. The evolution of the gas leak rates with the layer composition, i.e. from a pure spray powder layer (0/100 layer) up to a pure Tosoh powder layer (100/0 layer), can be described as a V-curve with a minimum value corresponding to the optimum composition. The optimum layer consists of 40 wt% of Tosoh powder and 60 wt% of spray powder (40/60 layer). For this optimum composition, an average helium leak rate of

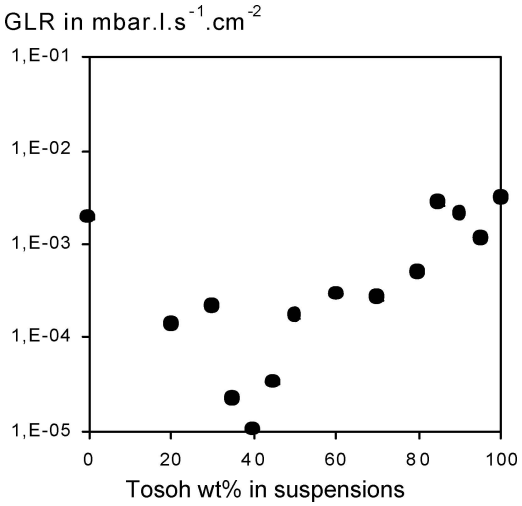

Figure 9 Helium leak rates of layers made of 800 spray powder/Tosoh 1240 powder mixtures.

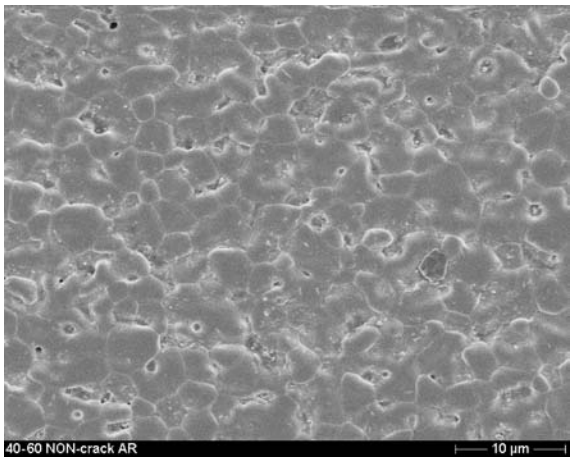

Figure 10 SEM top view of the 40/60 layer.

10^{-5}mbar $\cdot$ l $\cdot$ s^{-1} $\cdot$ cm^{-2} is observed through the co-fired layer. This gas leak rate is one order of magnitude lower than the expected value for an industrial application. An SEM micrograph of a layer made of this optimum composition is shown in Fig. 10. On this micrograph, it can be seen that the layer is much denser than layers made of pure calcined spray powder or pure Tosoh powder (micrographs shown in Figs 7 and 2, respectively).

To conclude this part, it can be noted that at this point that a protocol to prepare 5-μm-thick layers with efficient gastightness for anode-supported SOFCs has been found. From a practical point of view, this examination was quite successful. However, a complete interpretation of the gas leak rate evolution with layer composition still remains to be proposed. To achieve a satisfactory understanding, the layer green densities (depending on the compaction phenomenon of powders) and their sintering behaviour were analysed with regard to their sub micron-sized/micro-sized composition.

3.4. Interpretation and discussion of the results

The first interpretation study dealt with the green layer densities versus composition. Cross-section SEM analyses, which allowed the determination of the layer thickness for green density calculation, were carried out for three compositions: pure Tosoh, pure spray powder and 40/60 mixture. The procedure was repeated for three thicknesses of each composition (5, 15, 20 μm). Micrographs of the two extreme compositions are shown in Fig. 11. On these micrographs, a direct comparison between the two green electrolyte layers with the pre-calcined anode readiliy allows a rough evaluation of electrolytes green densities. Thus, one can clearly see that the layer made of spray powder is denser than the layer made of Tosoh powder. Indeed, the Tosoh layer is clearly less dense than the anode whereas the spray powder layer is clearly denser. The complete study of the evolution of the green density as a function of the composition is shown in Fig. 12. On this figure, open rhombuses represent experimental green densities determined for different thicknesses and full squares represent the average value determined for each composition. Firstly, it can be shown that the green density depends only on composition and not on layer thickness (the layer thickness was kept constant!). Secondly, the green layer density was found to continuously increase with the amount of spray powder used. The green densities are about 58% for the pure Tosoh layer and 68% for the pure spray powder layer. This can be explained by two factors: (i) the wider particle size distribution of the spray powder in comparison to the particle size distribution of the Tosoh powder, (ii) the shape factor of the spray particles (particles are perfectly spherical) which allows a better densification than for the Tosoh powder. Indeed, because a sphere is the most compact shape, spherical particles are known to lead to the densest stacking compared to non-sperical particles of the same particle size distrubution. This effect can be explained by enhanced friction and the stucking of the not ideal formed particles. Here, it can be added that compaction tests of zirconia balls (grinding media) were performed for comparison with the green density of the pure spray powder layer. For these tests, zirconia balls with different diameters (2, 3, 4, 5, and 10 mm) were used to roughly simulate the particle distribution of spray powder. Compacts with densities between 65 and 70% were obtained by pouring the balls into a beaker in bulk. This result shows that the high green density, calculated for pure spray powder layer (68%), thus appears reasonable.

The second interpretation study dealt with the sintering behaviour of "composite" pellets versus their composition. In all these studies, it was assumed that the sintering behaviour of pellets and layers of the same composition can be considered similar. Fig. 13 gives a general overview of the dilatometric curves recorded on pellets of different compositions. A continuous increase of the total shrinkage of the "composite" pellets is found as the amount of nano-sized powder increases. This increase of the total pellet shrinkage corresponds well to the higher final densities obtained (both green densities of pellets having been adjusted to 51–53%). Final densities after the same sintering of both pellets are listed in Table I. The final densities increase from about 85% for the pure Tosoh layer up to 95% for the pure spray powder layer.

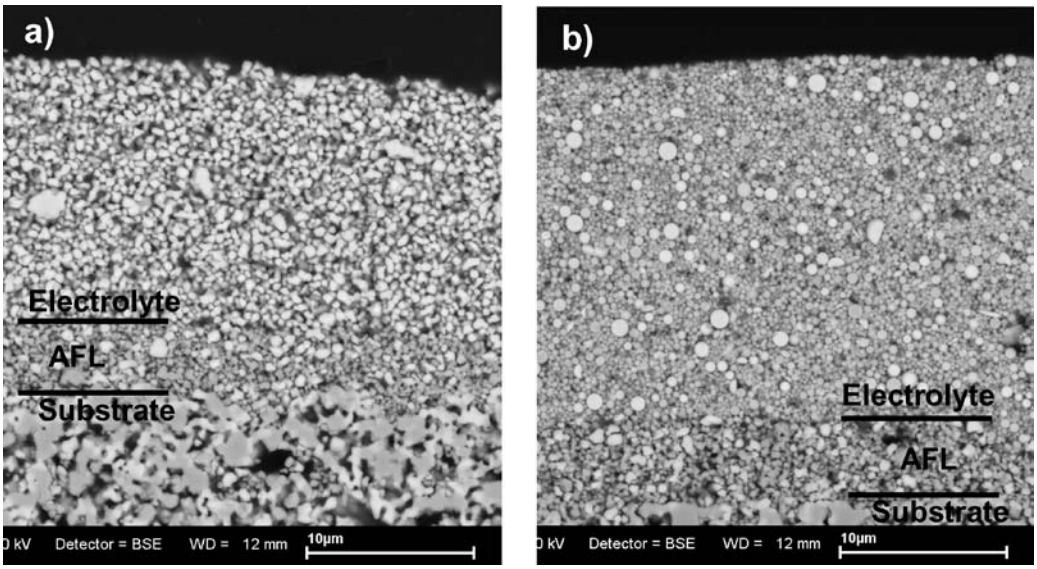

Figure 11 SEM cross views of green layers made of (a) Tosoh 1240 powder, (b) 800 spray powder; AFL: anode functional layer.

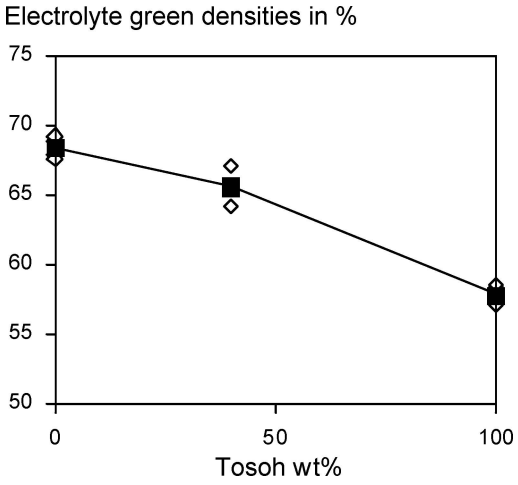

Figure 12 Calculated green densities of layers made of 800 spray powder/Tosoh 1240 powder mixtures.

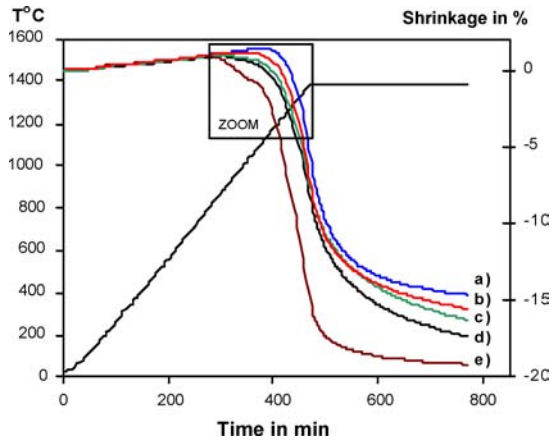

Figure 13 Dilatometric curves recorded on pellets made of Tosoh 1240 powder/800 spray powder mixtures (general view); (a) 100/0, (b) 60/40, (c) 40/60, (d) 20/80, (e) 0/100 pellets, respectively.

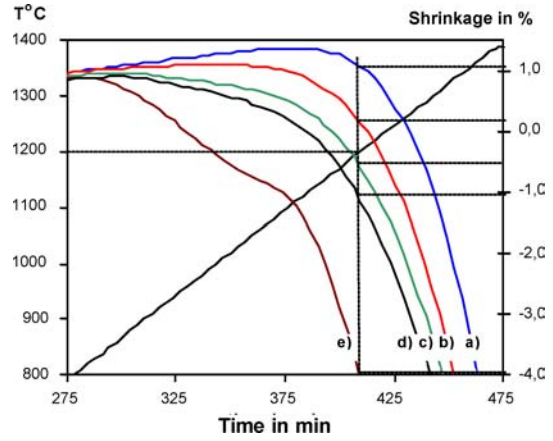

Figure 14 Dilatometric curves recorded on pellets made of 800 spray powder/Tosoh 1240 powder mixtures (zoom).

The green layer density study showed that the green density of layers increases with percentage of spray powder. Likewise, it is shown that the sintering of composite pellets is facilitated when the spray powder percentage increases. From these two studies, a continuous improvement of the density of "composite" sintered layers can only be explained because the amount of spray powder used increases up to an optimum value (which corresponds to the second branch of the V evolution of gas leak rate versus composition). Furthermore, because the increase of the amount of spray powders leads to a positive contribution for both green density and sintering activity, a subsequent strong improvement of sintered layer density can be explained by a synergy between these two effects. However, the fact that the evolution of the "composite" layer density is reversed beyond an optimal composition cannot be explained yet. To explain this optimum, we focused on the temperature of the start of sintering for each sample.

A zoom of the dilatometric curves corresponding to the starting of pellet shrinkage is presented in Fig. 14. From these curves it can be clearly seen that pellet shrinkage starts earlier and earlier when the amount of nano-sized powder increases. Furthermore, an additional step occuring at low temperature (about 900°C) can be noted for the pellet prepared from pure spray powder. If the shrinkage value of each sample is

TABLE I Density after sintering of pellets of different compositions.

Pellet composition	Density in %
100/0	95
80/20	92
60/40	88
40/60	84
0/100	85

analysed for 1200°C (the reader is assisted by the dotted lines in the firgure), very big differences are noticed between one sample and another. For the pellet made of pure Tosoh powder (the 100/0 pellet) no shrinkage has occurred at this temperature, which leads to a positive dilatation of 1%. It should be recalled that the shrinkage evolution of the Tosoh layer can be considered more or less similar to the shrinkage evolution of the substrate [13]. For 60/40, 40/60 and 20/80 composite pellets, shrinkages at 1200°C are about 0, 0.5 and 1%, respectively. For the pellet made of pure spray powder (the 0/100 pellet) the shrinkage is almost 4%. For temperatures above 1200°C, elastic contributions leading to a reduction of stress inside the layers can be neglected as was shown by Vaßen *et al.* [13]. Early shrinkage of the electrolyte film occurring below 1200°C is thus undoubtedly the principal cause of the appearance of cracks during co-firing treatment. From this hypothesis, the optimum final density found for the 40/60 sample can be explained by a critical shrinkage that must not be exceeded. For compositions containing more nano-sized powder, the differences in sintering activity between electrolyte films and anode substrate seem sufficient to cause the appearance of micro-cracks during the co-firing process. Thus, the appearance or not of cracks during co-firing seems to be very sensitive, since only a slight difference of shrinkage is noted between 40/60 and 20/80 pellets (please note that green densities of pellets and layers are not the same).

Finally, to complete this study, it was interesting to transfer the results obtained here to other mixtures of powders pre-sintered at different temperatures and thus having different sintering activity. Composite layers made from mixtures of a pre-calcined Tosoh powder at 800°C (Tosoh 800) and a pre-sintered Tosoh powder at 1240°C (Tosoh 1240) were studied. In comparison to the previous composite layers, the effect of the sub micron-sized particle shapes on the density of the green composite layer is suppressed here. Indeed, the granulometric distribution of Tosoh 800 powder in suspension is the same as for Tosoh 1240 suspension. However, the sintering activity of the Tosoh 800 powder can be considered approximately equivalent to the spray powders pre-calcined at 800°C. The gas leak rate results obtained on co-fired Tosoh 800/ Tosoh 1240 composite layers are presented in Fig. 15. The gas leak rates evolution versus the composite electrolyte composition can again be described as a V evolution as in the previous study. However, the gas leak rate for the optimal value is only approx. $10^{-4}\text{mbar} \cdot 1 \cdot \text{s}^{-1} \cdot \text{cm}^{-2}$, i.e., about one order of magnitude higher than for layers made of spray powder/Tosoh powder mixtures. This smaller optimum can be explained by a lack of improvement in green

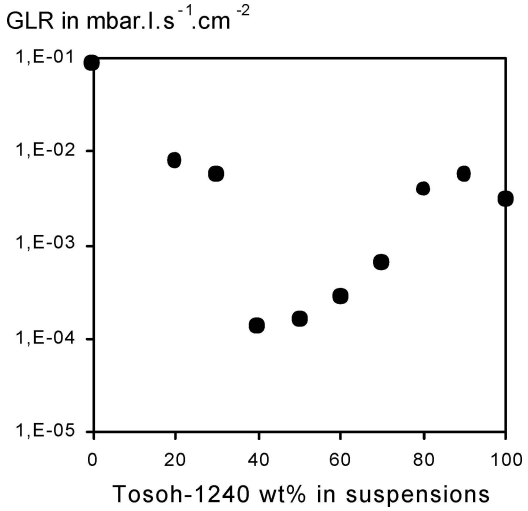

Figure 15 Helium leak rates of layers made of Tosoh 800 powder/Tosoh 1240 powder mixtures.

density with the amount of nano-sized powder in this last case. For Tosoh 800/Tosoh 1240 mixtures, only the effect of the sintering activity can play a role in the amelioration of the co-fired layer density.

4. Conclusion

The main result of this paper was the production of sufficiently gastight electrolyte layers of 5 μm thickness co-fired with an anode substrate for anode-supported SOFCs. To obtain satisfactory results, the electrolytes were prepared by slurry coating of micro-sized powder/nano-sized powder mixtures dispersed in suspension. An optimum powder mixture was found, which allowed the production of 5-μm-thick layers having a gas leak rate of $10^{-5}\text{mbar} \cdot 1 \cdot \text{s}^{-1} \cdot \text{cm}^{-2}$, i.e., one order of magnitude lower than the value required for industrial application. It was verified that the use of spray pyrolysis powder as a nano-sized powder for preparing a "composite" electrolyte was beneficial for the green density and the densification ability of the electrolyte. Indeed, the different particle size distribution of the spray pyrolysis powder (compared to the Tosoh material) in addition to their perfectly spherical shape improves the possibility of particle compaction and thus the green layer densities obtained. Furthermore, dilatometric experiments have shown that for sintered pellets made of spray powder very high density can be achieved in comparison with pellets made of micro-sized powder. However, the amount of nano-sized powder used must not exceed a critical value; beyond this value, too much early sintering activity of the layers leads to the appearance of film cracks during co-firing treatment.

Thus, it has been shown that for preparing a gastight and thin film on a porous substrate, under optimized conditions, the use of a sub micron-sized powder appears very positive.

Acknowledgements

The authors are grateful to G. Blass, A. Lemmens and Dr. D. Sebold for experimental assistance with the

slurry coating process and on granulometric distribution measurements, dilatometric and SEM analyses.

References

1. F. J. ROHR, P. HAGENMULLER and W. VANGOOL, "Solid Electrolytes" (Academic Press, New York, 1978) p. 431.
2. J. F. BAUMARD and P. ABELARD, *Adv. Ceram.* **24B** (1988) 71.
3. C. H. LEE, H. Y. LEE and S. M. OH, *Solid Sate Ionics* **98** (1997) 39.
4. L. KINDERMANN, D. DAS, D. BAHADUR, H. NICKEL and K. HILPERT, *Solid State Ionics* **106**(1/2) (1998) 165.
5. S. Y. BAE and S. W. WANG, *J. Mater. Res.* **13** (1998) 3224.
6. J. W. STEVENSON, P. F. HALLMAN, T. R. ARMSTRONG and L. A. CHICK, *J. Am. Ceram. Soc.* **80**(4) (1997) 909.
7. M. DOKIYA, *Solid State Ionics* **152/153** (2002) 383.
8. B. C. H. STEELE, in Proceedings of the 1st European SOFC Forum, edited by U. Bossel (Lucerne, Switzerland, 1994) p. 375.
9. N. H. MENZLER, R. FLECK, J. MERTENS, H. SCHICHL and H. P. BUCHKREMER, in Proceedings of the 5th European SOFC Forum, edited by J. P. P. Huijsmans Lucerne (Switzerland, 2002) p. 156.
10. D. STOEVER, H. P. BUCHKREMER and J. P. P. HUIJSMANS, in Handbook of Fuel Cells: Fundamental, Technology and Applications, edited by W. Vielstich, H. A. Gasteiger and A. Lamm (John Wiley & Sons Ltd., Chichester, U.K., West Sussex, 2003) p. 1015, vol. 4.
11. F. TIETZ, H.-P. BUCHKREMER and D. STÖVER, *Solid State Ionics* **152/153** (2002) 373.
12. P. BATFALSKY, H. P. BUCHKREMER, D. FRONING, F. MESCHKE, H. NABIELEK, R. W. STEINBRECH and F. TIETZ, in Proceedings of the 3rd International Fuel Cell Conference, Nagoya, Japon (1999) p. 349.
13. R. VASSEN, R. W. STEINBRECH, F. TIETZ and D. STOEVER, in Proceedings of the 3rd European SOFC Forum, edited by P. Stevens, (Oberrohrdorf, Switzerland 1998) p. 156.
14. S. DE SOUZA, S. J. VISCO and L. C. DE JONGHE, *Solid State Ionics* **98** (1997) 57.
15. N. H. MENZLER, E. DJURADO, A. GEDANKEN, H. P. BUCHKREMER and D. STOEVER, in Proceedings of the 5th European SOFC Forum, edited by J. P. P. Huijsmans Lucerne, (Switzerland 2002) p. 171.
16. M. MOSKOVITS, B. G. RAVI and R. CHAIM, *NanoStructured Materials* **11**(2) (1999) 179.
17. R. CHAIM and G. BASAT *Mater. Lett.* **35** (1998) 245.
18. Y. J. LENG, S. W. CHAN, K. A. KHOR, S. P. JIANG and P. CHANG, *J. Power Sour.* **117** (2003) 26.
19. X. J. CHEN, K. A. KHOR, S. H. CHAN and L. G. YU, *Mater. Sci. Engng. A* **335** (2002) 246.
20. N. H. MENZLER, D. LAVERGNAT, F. TIETZ, E. SOMINSKI, E. DJURADO, G. PANG, A. GEDANKEN and H. P. BUCHKREMER, *Ceram. Int.* **29**(6) (2003) 619.
21. E. DJURADO and E. MEUNIER, *J. Sol. State Chem.* **141** (1998) 191.
22. R. N. BASU, G. BLASS, H. P. BUCHKREMER, D. STOEVER, F. TIETZ, E. WESSEL and I. C. VINKE, in Proceedings of the 7th International Symposium on Solid Oxide Fuel Cell, edited by H. Yokokawa and S. C. Singhal (Tsukuba, Japan 2001) p. 995.
23. W. A. MEULENBERG, N. H. MENZLER, H. P. BUCHKREMER and D. STOEVER, *Ceram. Trans.* **127** (2002) 99.
24. M. GAUDON, N. H. MENZLER and E. DJURADO, Accepted for publication in *Ceram. Int.* **30** (2004) 2235; available online via Science Direct since april 21st 2004.

Received 10 March 2004
and accepted 10 February 2005